arXiv:1406.3471v1 [astro-ph.SR] 13 Jun 2014

Chapter 5
Blue Straggler Stars in Globular Clusters: a powerful tool to probe the internal dynamical evolution of stellar systems

Francesco R. Ferraro, Barbara Lanzoni, Emanuele Dalessandro, Alessio Mucciarelli, and Loredana Lovisi

5.1 Introduction

Blue straggler stars (BSSs) in globular clusters (GCs) are commonly defined as those stars located along an extrapolation of the main sequence (MS), in a region brighter and bluer (hotter) than the turnoff (TO) point, in the optical colour-magnitude diagram (CMD; see Fig. 5.1). They were first discovered by Sandage [70] in the external region of the Galactic GC M3. Their origin has been a mystery for many years and the puzzle of their formation is not completely solved yet.

The BSS location in the CMD suggests that they are more massive than the current cluster population (Fig. 5.1; this is also confirmed by a few mass measurements, e.g., [74, 35]). However, GCs are completely devoid of gas and any recent star formation event can be realistically ruled out. Hence the BSS origin should be searched in some mechanisms able to increase the initial mass of single stars in a sort of *rejuvenation process*. The BSS formation mechanisms are not completely understood yet, but the main leading scenarios, at present, are mass transfer (MT) processes between binary companions [58, 82], possibly up to the complete coalescence of the binary system, or the merger of stars induced by collisions (COLL; [37]). Being more massive than the average cluster stars, BSSs suffer from the effect of dynamical friction, that makes them sink towards the cluster centre [53, 32]. In turn, the frequent stellar interactions occurring in the ultra-dense cores of Galactic GCs can promote both the formation and the hardening of binary systems, thus contributing to generate MT-BSSs. All these considerations clearly show that BSSs represent a crucial link between standard stellar evolution and GC internal dynamics (see [3, 32], and references therein).

Francesco R. Ferraro et al.
Dipartimento di Fisica e Astronomia, Università degli Studi di Bologna, Via Ranzani 1, I–40127 Bologna, Italy, e-mail: francesco.ferraro3@unibo.it

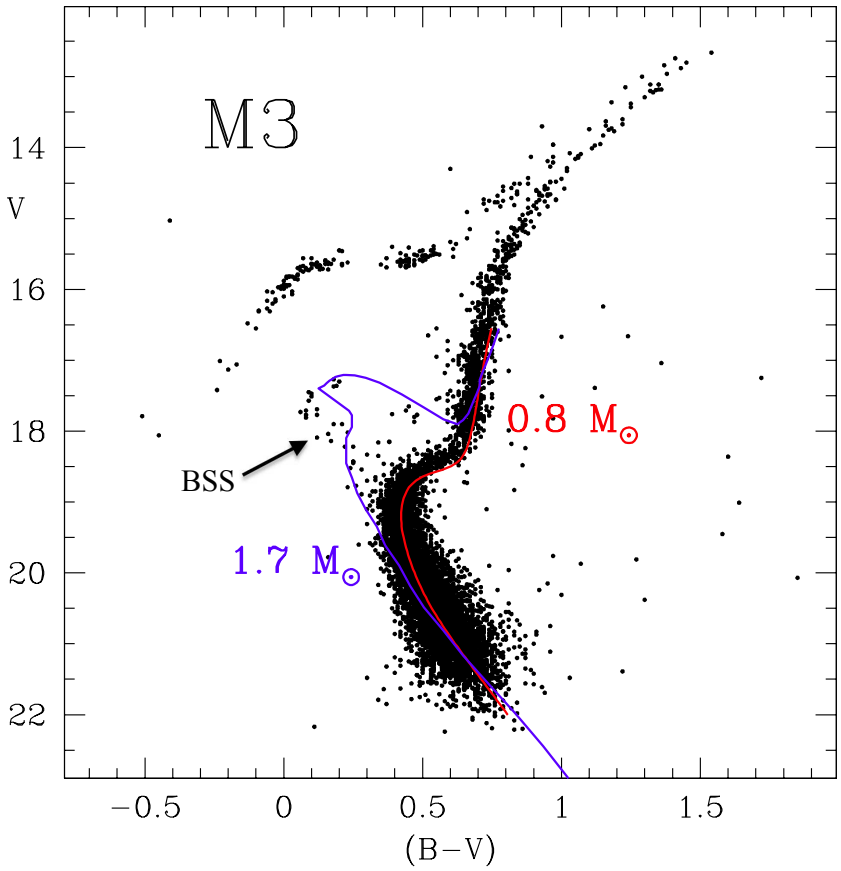

Fig. 5.1 Optical CMD of the globular cluster M3, with the location of BSSs indicated by the arrow. The theoretical track corresponding to 0.8 $M_{\odot}$ reproduces well the main evolutionary sequences of the cluster, while BSSs populate a region of the CMD where core hydrogen-burning stars of ~ 1.7 $M_{\odot}$ are expected. From [9].

5.2 BSS Specific Frequency and Primordial Binary Fraction

The observational and interpretative scenario of BSSs has significantly changed in the last years. In fact, for a very long time (almost 40 years) since their discovery (see Chap. 2), BSSs have been detected only in the outer regions of GCs, or in relatively loose clusters. This generated the idea that low-density environments were their *natural habitats*. However, starting from the early '90, high spatial resolution facilities allowed to properly image and discover BSSs also in the highly-crowded

central regions of dense GCs (see the case of NGC 6397; [2]), thus demonstrating that the previous conviction was just due to an observational bias. In particular, the advent of the *Hubble Space Telescope* (HST) represented a real turning point in BSS studies, thanks to its unprecedented spatial resolution and imaging/spectroscopic capabilities in the ultraviolet (UV). Indeed, the pioneering observations of the central regions of 47 Tucanae [64, 34] and M15 [21], by means of the HST opened a new perspective in the study of BSSs, definitely demonstrating that they also (preferentially) populate high-density environments.

Based on these observations, the first catalogs of BSSs have been published (e.g., [33, 71]) and the first comparisons among different clusters have been attempted [23]. In order to perform meaningful comparisons, various definitions of BSS specific frequencies have been proposed over time. Ferraro and colleagues [22] introduced the "double normalised ratio", defined as:

$$R_{\rm BSS} = \frac{(N_{\rm BSS}/N_{\rm BSS}^{\rm tot})}{(L^{\rm sampled}/L_{tot}^{\rm sampled})}, \tag{5.1}$$

where $N_{\rm BSS}$ is the number of BSSs counted in a given cluster region, $N_{\rm BSS}^{\rm tot}$ is the total number of BSSs observed, and $L^{\rm sampled}/L_{tot}^{\rm sampled}$ is the fraction of light sampled in the same region, with respect to the total measured luminosity. The same ratio can be defined for any post-MS population. Theoretical arguments [68] demonstrate that the double normalised ratio is equal to unity for any population (such as red giant branch and horizontal branch stars, RGB and HB, respectively) whose radial distribution follows that of the cluster luminosity. Other definitions of the BSS specific frequency adopted in the literature are: $S4_{\rm BSS} = N_{\rm BSS}/L_s$, where $N_{\rm BSS}$ is the number of BSSs and L_s is the sampled luminosity in units of 10^4 $L_\odot$ [23]; $F_{\rm BSS} = N_{\rm BSS}/N_{\rm bright}$, where $N_{\rm bright}$ is the number of all the stars brighter than two magnitudes below the HB level [8]; $F_{\rm pop}^{\rm BSS} = N_{\rm BSS}/N_{\rm pop}$ [26], where $N_{\rm pop}$ is the number of stars belonging to a cluster "normal" population adopted as reference (generally the HB population, or a segment of the RGB or MS). Besides the different definitions, all these normalisations account for the different cluster richness (i.e, total luminosity or mass). However, as discussed in [23], particular caution is needed when looking for correlations among BSS specific frequencies and cluster structural parameters, since the concentration parameter and central density are intrinsically related to the cluster luminosity (see, e.g., [18]); hence spurious correlations can emerge simply because of the BSS "normalisation".

The largest compilations of BSSs to date have been collected for nearly 60 Galactic GCs surveyed with the HST/WFPC2 [66, 45, 63], and for 35 clusters [46] observed within the HST/ACS *Survey of Galactic Globular Clusters* [72]. These compilations, together with deep investigations in open clusters, dwarf spheroidals, and the Galactic field (see Chap. 3, 4, and 6 in this book), have significantly contributed to form the nowadays largely accepted idea that BSSs are a stellar population common to any stellar system.

With the aim of understanding how BSSs form and if their formation mechanisms depend on some cluster physical properties, the most recent catalogs have been used

to search for correlations between the BSS specific frequency (or number), and several parameters tracing the cluster structure (as luminosity, mass, central density, etc.), as well as for correlations with the collision rate and binary fraction (for recent results, see Chap. 9). Though not conclusive, this approach has provided a number of interesting results. For instance, no correlation has been found with the collisional parameter [66, 16, 45], while a strong correlation has been revealed between the number of BSSs in cluster cores and the core mass [39, 47]. These facts have been interpreted as the evidence of a binary (instead of a collisional) origin of BSSs, even in the densest environments, like the centre of post-core collapsed (PCC) clusters [39]. However, the fraction of binary systems in a sample of 59 GCs has been recently estimated from the distribution of stars along the "secondary" MS [61], thus allowing to explore directly any possible correlation between the fraction/number of BSSs and that of binaries. By using a sub-sample of 24 GCs, Milone et al. [61] found a nice correlation between the BSS specific frequency and the binary fraction in cluster cores. This has been confirmed also by Leigh et al. [47], who, however, obtain a much stronger correlation between the number of core BSSs and the cluster core mass. Interestingly, in Milone et al. [61] plot, PCC clusters lie well outside the relation. This likely reflects the role that internal dynamics plays on the binary and BSS content of GCs. In fact, binary systems are subject to frequent dynamical interactions with other binaries, single stars and even multiple systems. These interactions can either bring to stellar collisions, or significantly alter the physical properties of binaries, even promoting mass transfer activity. Hence, binaries and interactions play a crucial role in both the MT and the COLL scenarios and it is probably impossible to separate the two effects just on the basis of the observed binary fraction. An exception could be represented by low density environments, where the efficiency of dynamical interactions is expected to be negligible. Very interestingly, indeed, a clear correlation between the binary and the BSS frequency has been found in a sample of 13 low density GCs ($\log \nu_0 < 3$ in units of $L_\odot/pc^3$; see Fig. 5.2 and [78]). This is the cleanest evidence that the unperturbed evolution of primordial binaries is the dominant BSS formation process in low-density environments (also consistently with the results obtained in open clusters; e.g., [57]).

5.3 The Ultraviolet Route to Study BSS

The systematic study of BSSs in the visible-light bands, especially in the central regions of high density clusters, is intrinsically difficult and remains problematic even when using HST. This is because the optical emission of old stellar populations is dominated by cool, bright giants. Hence, the observation of complete samples of (faint) hot stars (as BSSs, other by-products of binary system evolution, extreme blue horizontal branch stars, etc.) is quite problematic in this plane. *It is like trying to make a complete census of fire-flies, while having a clump of large light-bulbs just in front of us. In order to secure a proper counting of fire-flies one needs to switch off the lights, first!*. Moreover, in the visible-light plane, BSSs can be easily

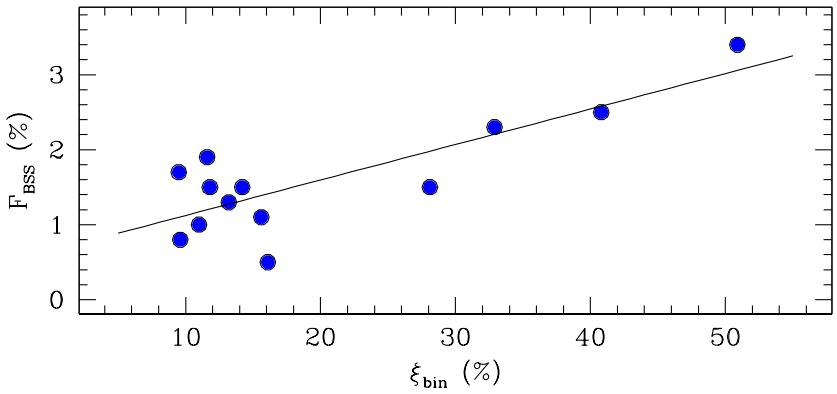

Fig. 5.2 BSS specific frequency as a function of the core binary fraction measured in a sample of low-density GCs. The best-fit linear correlation is also plotted (solid line). From [78].

mimicked by photometric blends of subgiant branch (SGB) and RGB stars. Instead, at ultraviolet (UV) wavelengths RGB stars are very faint, while BSSs are among the brightest objects. In particular, in the UV plane BSSs are much more easily recognisable, since they define a narrow, nearly vertical sequence spanning a ~ 3 mag interval (see Fig. 5.3). In the mean time, BSS-like blends are much less severe at these wavelengths because of the relative faintness of SGB and RGB stars. Indeed, the $(m_{255}, m_{255} - m_{336})$ plane has been found to be ideal for selecting BSSs even in the cores of the densest GCs.

The UV exploration of the very central region of M3 (see [24], hereafter F97; see also Fig.5.4] brought to the discovery of a substantial population of BSSs, at odds with the depletion claimed by Bolte, Hesser & Stetson [8]. Since then, the central regions of a number of GCs have been explored in the UV to search for BSSs: this systematic approach allowed putting the BSS study into a more quantitative basis than ever before. Indeed a number of interesting results have been obtained from cluster-to-cluster comparisons (see Fig. 5.5). Of course the UV approach strongly favours the observation of hot objects, like HB stars (see Fig. 5.3). Hence the HB becomes the ideal reference population for the definition of the BSS specific frequency ($F_{\rm HB}^{\rm BSS}$) at these wavelengths.

By using appropriate observations in the UV (Fig. 5.5), Ferraro et al.[26] presented a comparison of the BSS populations in the central regions of 6 clusters (namely NGC 288, M92, M3, M13, M80, and M10) characterised by different structural parameters. The BSS specific frequency ($N_{\rm BSS}/N_{\rm HB}$) has been found to largely vary from cluster to cluster, from 0.07 to 0.92, and it does not seem to be correlated with central density, total mass, velocity dispersion, or any other obvious cluster property (see also [66]). On the other hand, this study pointed out peculiar cases that statistical approaches (as those presented, e.g., by [66]) did not bring into evi-

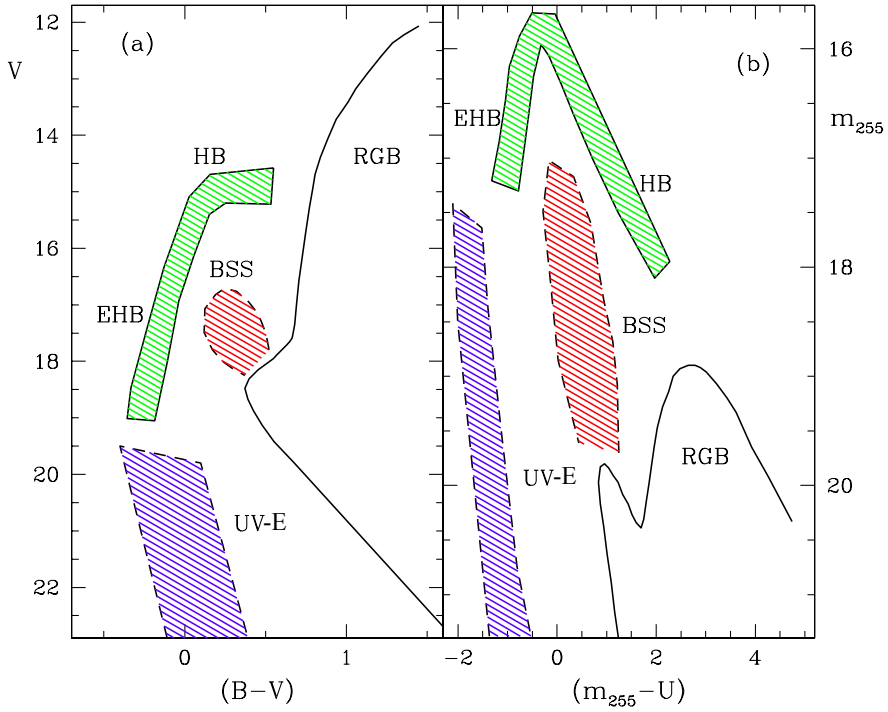

Fig. 5.3 Sketch of the stellar evolutionary sequences in the optical (left panel) and in the UV (right panel) CMDs. The loci of RGB, BSS, HB, extreme-HB stars (EHB) and stars with UV excess are marked.

dence. "Twin" clusters like M3 and M13 have been found to harbour quite different BSS populations: the specific frequency in M13 is the lowest ever measured in a GC (0.07), and it turns out to be 4 times lower than that measured in M3 (0.28). *What is the origin of this difference?* We [26] suggested that it could be related to their binary content; in particular the paucity of BSSs in M13 could be due either to a quite poor population of primordial binaries, or to the fact that most of them were destroyed during the cluster evolution. Indeed the fraction of binaries recently measured in the central regions of these two clusters [61] confirms a significant difference ($f_{\rm bin} = 0.027$ for M3, and $f_{\rm bin} = 0.005$ for M13), thus supporting the hypothesis that this is the origin of the different BSS content. One of the most interesting result is that the largest BSS specific frequency has been found in two GCs which are at the extremes of the central density values in the analysed sample: NGC 288 and M80, with the lowest and the highest central density, respectively ($\log\rho_0 = 2.1$ and 5.8, in units of $M_\odot/pc^3$). This suggests that the two formation channels can have comparable efficiency in producing BSSs in the respective most favourable environment.

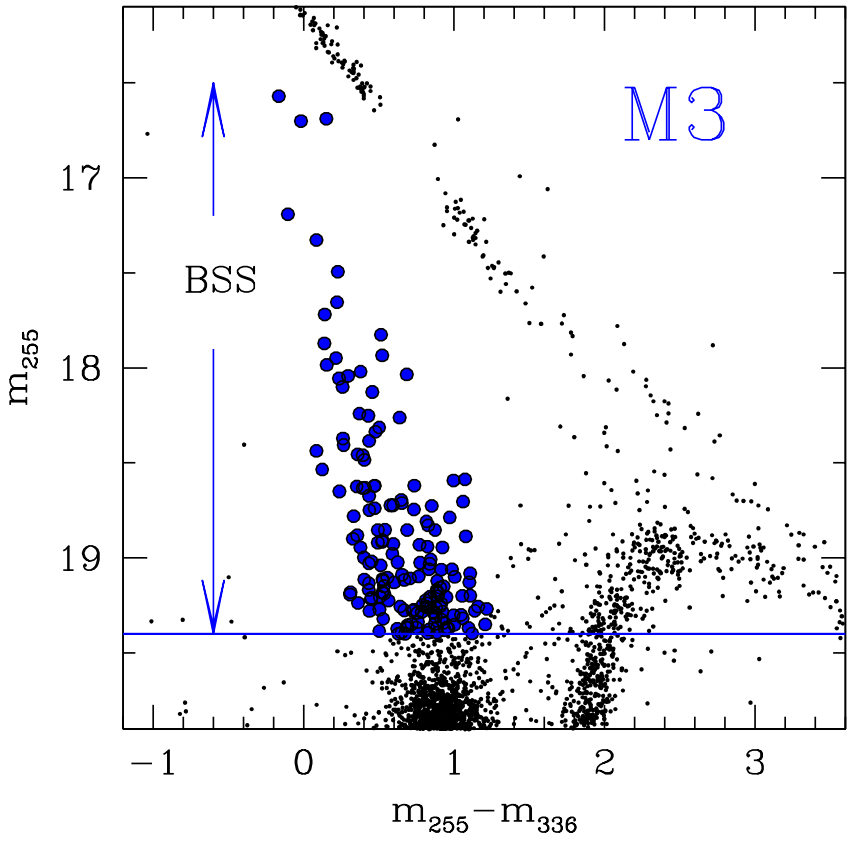

Fig. 5.4 BSS in the UV: the case of M3. The horizontal line at $m_{255} = 19.4$ is the assumed BSS limiting magnitude, corresponding to $\sim 5\sigma$ above the turnoff level. From [24].

5.4 The Discovery of the Double BSS Sequence

While the proposed BSS formation mechanisms could be separately at work in clusters with different densities [23, 25], a few pieces of evidence are now emerging suggesting that they could also act simultaneously within the same cluster. Indeed the discovery of a double BSS sequence in M30 ([31], hereafter F09) indicates that this can be the case.

By using an exceptional set of 44 high-resolution images obtained with the HST-WFPC2, F09 obtained a very high-precision CMD of the central region of the Galactic GC M30. The CMD revealed the existence of two well-separated and almost parallel sequences of BSSs (Fig. 5.6). The two sequences are similarly populated,

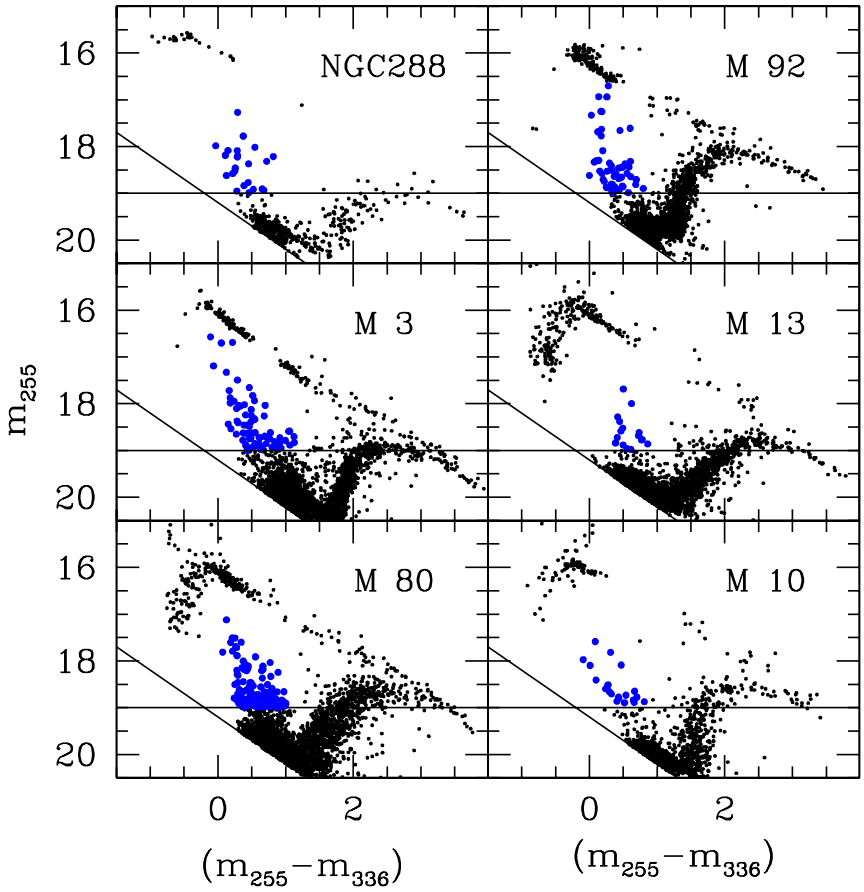

Fig. 5.5 UV CMDs of six different globular clusters (see labels), with the BSS populations highlighted as blue circles. The horizontal line marks the magnitude limit adopted for the BSS selection. From [26].

consisting of 21 and 24 stars, respectively. *This is the very first time that such a feature has been detected in any stellar system, and it could be the signature of the cluster core collapse imprinted onto the BSS population.*

The comparison with evolutionary models of BSS formed by direct collisions of two MS stars [77] shows that the blue-BSS sequence is well fit by collisional isochrones with ages of $1-2$ Gyr (black solid lines in Fig. 5.7). Instead, the red-BSS population is far too red to be properly reproduced by collisional isochrones of any age, and its origin should therefore be different. Binary evolution models [79] have shown that during the mass-transfer phase (which can last several Gyr, i.e., a

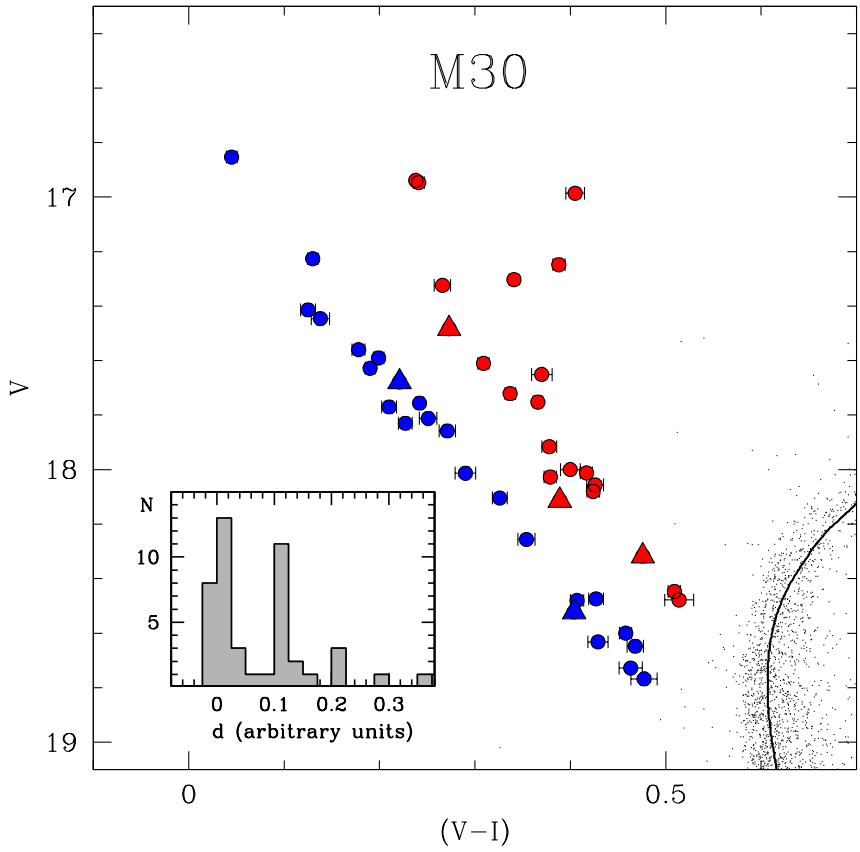

Fig. 5.6 Optical CMD of M30 zoomed in the BSS region. The two distinct sequences of BSSs are highlighted as blue and red symbols. The inset shows the distribution of the geometrical distances of BSSs from the straight line that best fits the blue BSS sequence. Two well-defined peaks are clearly visible, confirming that the two sequences are nearly parallel to each other. From [31].

significant fraction of the binary evolution time-scale), the binary population defines a sort of "low-luminosity boundary" located ~ 0.75 mag above the zero-age MS in the BSS region. This is just where the red-BSS sequence is observed (red dashed line in Fig. 5.7). Hence, the BSS along the red-sequence could be binary systems still experiencing an active phase of mass-exchange.

Due to the normal stellar evolution, all BSSs will evolve toward the RGB phase. In particular, the evolved blue-BSSs will populate the region between the two observed sequences and fill the gap. Hence, the fact that two well-separated chains of stars are observed supports the hypothesis that both the blue- and the red-BSS populations have been *generated by a recent and short-lived event, instead of a con-*

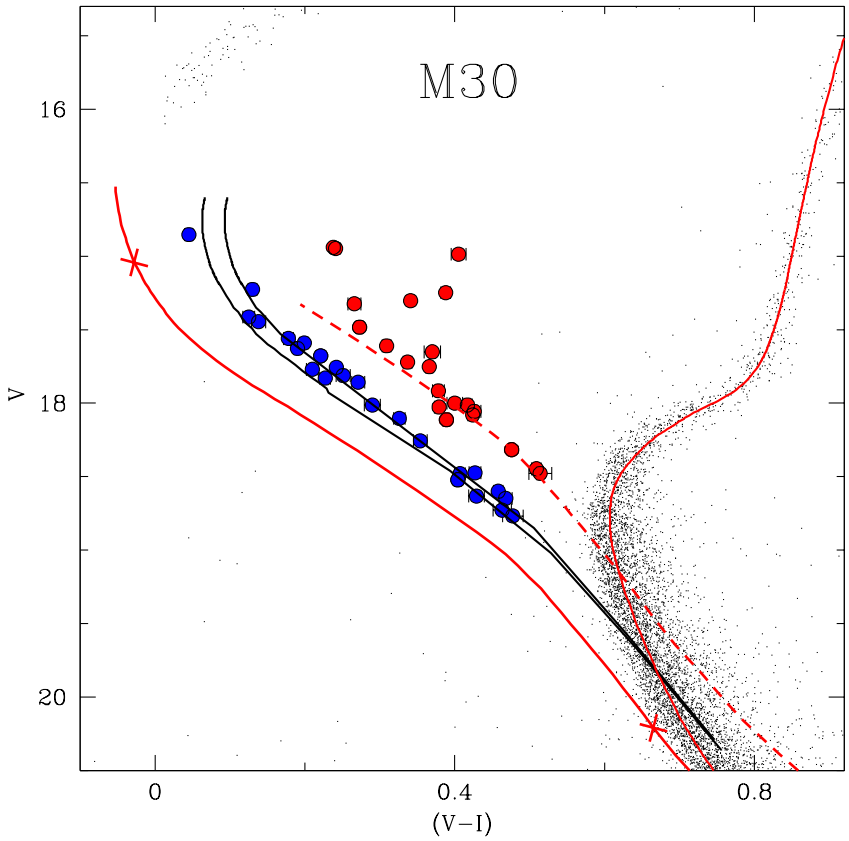

Fig. 5.7 Magnified portion of the CMD of M30. The solid black lines correspond to the collisional isochrones of 1 and 2 Gyr, respectively, which accurately reproduce the blue BSS sequence. The solid red lines correspond to the single-star isochrones of 13 Gyr (well fitting the main cluster evolutionary sequences) and 0.5 Gyr (representing the reference cluster zero-age main sequence, ZAMS). The two crosses mark the respective positions of a 0.8 $M_{\odot}$ star and a 1.6 $M_{\odot}$ star along the ZAMS. The dashed red line corresponds to the ZAMS shifted by 0.75 mag, marking the lower boundary of the locus occupied by mass-transfer binary systems. This line well reproduces the red BSS sequence. From [31].

tinuous formation process. Quite interestingly, M30 is classified as a PCC cluster in the original compilation of Djorgovski & King [19], and F09 confirmed this finding by carefully re-determining the cluster density profile from deep HST images and detecting a steep power-law cusp in the innermost 5″–6″($\sim$ 0.2 pc). During the core collapse phase the central stellar density rapidly increases, bringing to a concomitant enhancement of gravitational interactions (in fact, the collisional parameter scales as $\Gamma \propto \rho_0^{1.5} r_c^2$, where r_c is the core radius). In turn, these can trigger

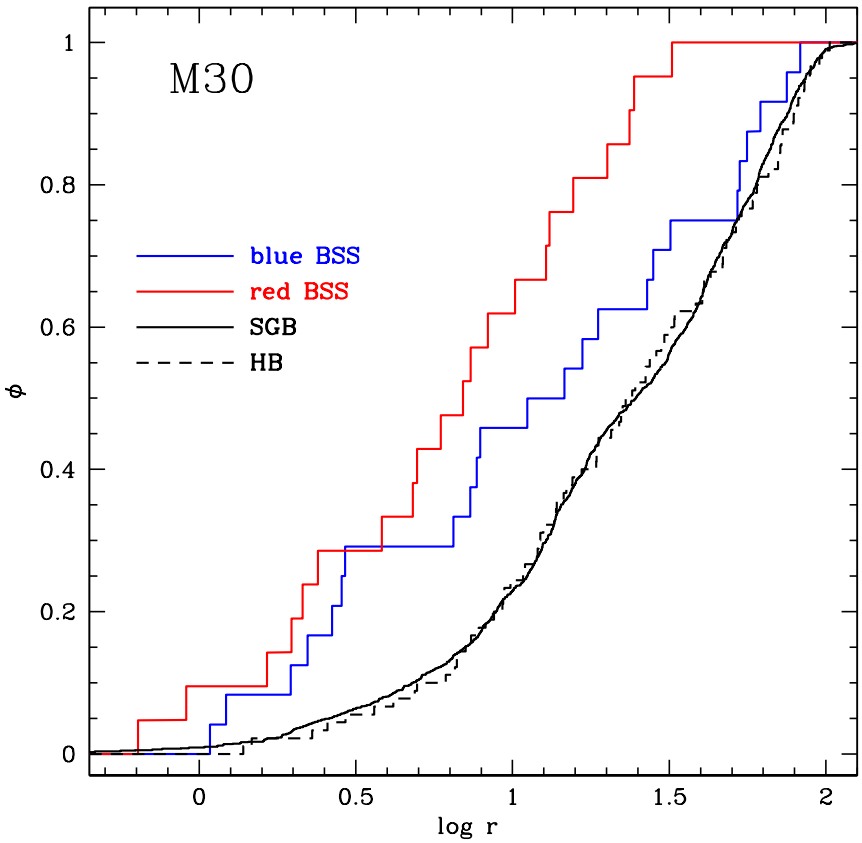

Fig. 5.8 Cumulative radial distributions of red BSSs (red line) and blue BSSs (blue line), as function of the distance from the cluster centre. The distributions of subgiant branch stars (solid black line) and horizontal-branch stars (dashed black line) are also plotted, for comparison. From [31].

the formation of new BSSs, both via direct stellar collisions and via mass transfer activity in dynamically shrunk binary systems. All together these considerations support a scenario where the two observed BSS populations are generated by the same dynamical event (the core collapse): the blue-BSSs arose from the enhanced stellar collision activity, while the red-BSSs are the result of the evolution of binary systems which first sank into the cluster center because of the dynamical friction (or they were already present into the cluster core), and then have been driven into the mass-transfer regime by hardening processes induced by gravitational interactions during the core collapse phase. According to this scenario, *the double BSS sequence detected in M30 dates the occurrence of the core collapse event back to 1–2 Gyr ago. If the proposed scenario is correct, this discovery opens the possibility of defining*

a powerful "clock" to date the occurrence of this dramatic event in a star cluster history (see also Section 5.6).

Additional clues in favour of a different formation history for the BSSs belonging to the two sequences are suggested by their central concentration and specific frequency. The red-BSSs are more centrally segregated than the blue ones (Fig. 5.8), with no red-BSSs observed at $r > 30''$ (~ 1.3 pc) from the cluster center. Moreover, the value of the BSS specific frequency with respect to HB stars varies significantly over the cluster extension, reaching the surprising value of ~ 1.55 when only the central cusp of the star density profile ($r < 5'' - 6''$) is considered. This is the highest BSS specific frequency measured in any GC [26], and it further supports the possibility that in M30 we are observing the effect of an enhanced gravitational interaction activity on single and binary stars.

The proposed picture leads to a testable observational prediction: the red-BSS sequence should be populated by binaries with short orbital periods. A recent paper [39] suggested that the dominant BSS formation channel is the evolution of binary systems, independently of the dynamical state of the parent cluster. The double BSS sequence in M30 possibly shows that binary evolution alone does not paint a complete picture: dynamical processes can indeed play a major role in the formation of BSSs. Interestingly, preliminary indications of double BSS sequences have been collected for two additional clusters: M15 (Beccari et al. 2014, in preparation) and NGC 362 [15]. Moreover, detailed spectroscopic investigations are certainly worth performing to obtain a complete characterisation of the BSS properties (orbital periods, rotation velocities, etc.). In this respect particularly promising is the search for the chemical signature of the MT process (see Section 5.8) for the BSSs along the red sequence.

5.5 The BSS Radial Distribution

M3 has played a fundamental role in the BSS history: not only it is the system where BSSs have been first identified [70], but also where their radial distribution has been studied over the entire cluster extension for the first time (F97). In fact by combining UV HST observations of the cluster central region (F97) and wide field ground-based observations in the visible-light bands [22, 9], F97 presented the BSS radial distribution of M3 out to $r \sim 6'$. The result was completely unexpected: BSSs appeared to be more centrally concentrated than RGB stars in the cluster central regions, and less concentrated in the outskirts. The result is shown in Fig. 5.9 and it clearly shows that the radial distribution of BSSs in M3 is bimodal: it reaches a maximum in the centre of the cluster, shows a clear-cut dip in the intermediate region (at $100'' < r < 200''$), and rises again in the outer region.

Sigurdsson, Daviest & Bolte [75] suggested that the bimodal BSS distribution observed in M3 could be explained by assuming that all BSSs formed in the core by direct collisions (thus creating the central peak of the distribution) and some of them were kicked out from the centre by the recoil of the interactions. Those BSSs

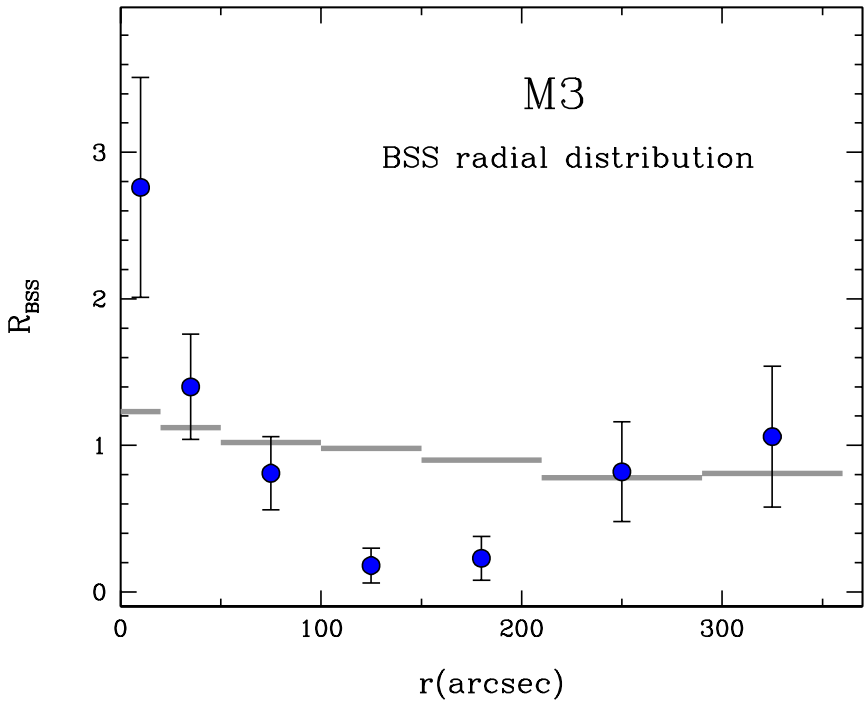

Fig. 5.9 Bimodal radial distribution of BSSs in M3. Blue dots mark the value of the BSS double normalised ratio as defined in eq. (5.1), computed at various distances from the cluster centre, the gray segments mark the double normalised ratio of HB stars. From [24].

ejected to a few core radii rapidly drifted back to the centre of the cluster due to mass segregation (thus contributing to the central BSS concentration and generating the paucity of BSSs at intermediate distances of a few core radii). BSSs affected by more energetic recoils would have been kicked out to larger distances and, since they require much more time to drift back toward the core, they may account for the overabundance of BSSs observed in the cluster outskirts. However, Monte-Carlo dynamical simulations [53, 54] demonstrated that BSSs kicked out from the core either are lost from the cluster, or sink back to the centre in 1–2 Gyr only. Hence, the observed BSS bimodal distributions cannot be explained with a purely collisional population, and to accurately reproduce the external upturn of the distribution it is necessary to assume a sizable fraction ($\sim 20-40\%$) of MT-BSSs, generated in the peripheral regions where primordial binaries can evolve in isolation and experience mass transfer processes without suffering significant interactions with other cluster stars.

While the bimodality detected in M3 was considered for years to be *peculiar*, more recent results demonstrated that this is not the case. In fact, the same observational strategy adopted by F97 in M3 has been applied to a number of other clusters, and bimodal distributions have been detected in the majority of cases (~ 15) studied so far. Examples can be found in: 47 Tuc [28] , NGC 6752[69], M55 [81, 42], M5 [80, 40], NGC 6388 [13], M53 [5]. Only a few exceptions are known: M79 and M75, which do not present any external upturn [41, 12], and three clusters (ω Centauri, NGC 2419 and Palomar 14) showing a completely flat BSS radial distribution, totally consistent with that of the reference population ([29, 14, 6], respectively). The last three cases deserve a specific comment. The flat behaviour discovered in these clusters suggests that the BSS radial distribution is not yet significantly altered by stellar interactions and by the dynamical evolution of the cluster. *Indeed, this is the cleanest evidence of the fact that these systems are not fully relaxed yet, even in the central regions*. We emphasise that this result is much more solid than any other estimate of mass segregation in these stellar systems. In fact, the degree of mass segregation is usually evaluated from star number counts along the MS, down to quite faint magnitudes where incompleteness biases can be severe (see, e.g., [1, 38]). Instead the computation of the BSS specific frequency refers to much brighter objects, as BSS and TO/RGB/HB stars.

5.6 Setting the Dynamical Clock for Stellar Systems

The entire database of available BSS radial distributions has been analysed by us ([32], hereafter F12). Such a dataset contains 21 GCs with very different structural properties (hence possibly at different stages of their dynamical evolution), but with nearly the same chronological age (12-13 Gyr; [56]), with the only exception of Palomar 14 which formed ~ 10.5 Gyr ago [20]. While significant cluster-to-cluster variations were already known, F12 discovered that once the radial distance from the centre is expressed in units of the core radius (thus to allow a meaningful comparison among the clusters), GCs can be efficiently grouped on the basis of the shape of their BSS radial distribution, and at least three families can be defined:

- *Family I* – the radial distribution of the BSS double normalised ratio ($R_{\rm BSS}$) is fully consistent with that of the reference population ($R_{\rm pop}$) over the entire cluster extension (see Fig. 5.10);
- *Family II* – the distribution of $R_{\rm BSS}$ is incompatible with that of $R_{\rm pop}$, showing a significant bimodality, with a central peak and an external upturn. At intermediate radii a minimum is evident and its position ($r_{\rm min}$) can be clearly defined for each sub-group (see Fig. 5.11);
- *Family III* – the radial distribution of $R_{\rm BSS}$ is still incompatible with that of the reference population, showing a well defined central peak with no external upturn (see Fig. 5.12).

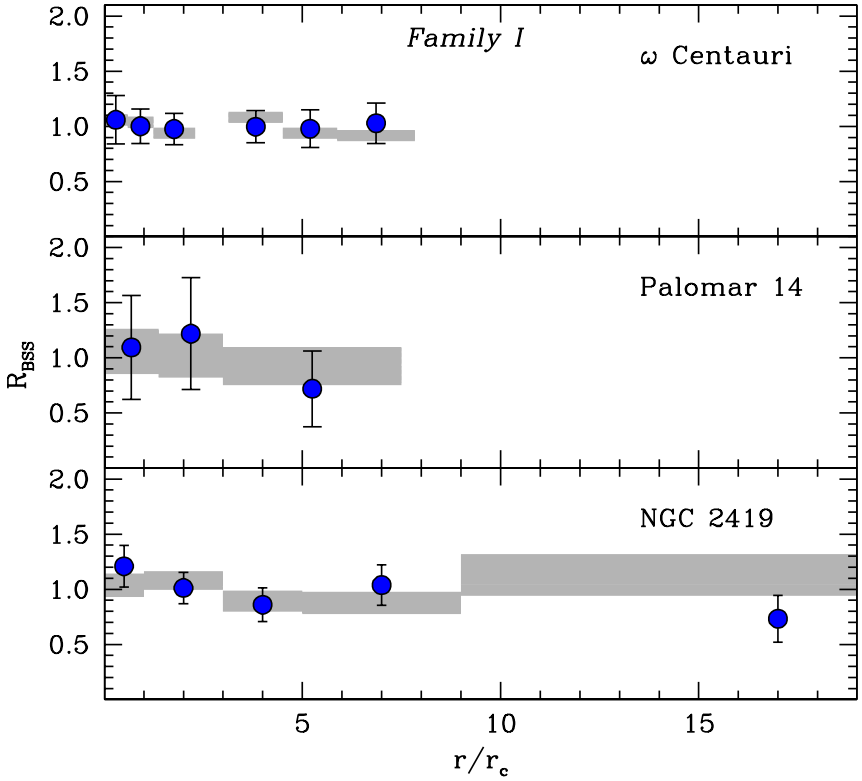

Fig. 5.10 BSS radial distribution observed in ω Centauri, Palomar 14 and NGC 2419, with the blue circles marking the values of $R_{\rm BSS}$, defined in eq. (5.1). The distribution of the double normalised ratio measured for RGB or HB stars is also shown for comparison (grey strips). The BSS radial distribution is flat and totally consistent with that of the reference population, thus indicating a low degree of dynamical evolution for these three GCs (*Family I*). From [32].

Which is the physical origin of these distributions? Previous preliminary analysis [53, 54, 40, 41] of a few clusters indicated that BSSs generated by stellar collisions mainly/only contribute to the central peak of the distribution, while the portion beyond the observed minimum is populated by MT-BSSs which are evolving in isolation in the cluster outskirt and have not yet suffered the effects of dynamical friction (see Sect. 5.5). Overall, the BSS radial distribution is primarily modelled by the long-term effect of dynamical friction acting on the cluster binary population (and its progeny) since the early stages of cluster evolution. In fact, what we call MT-BSS today is the by-product of the evolution of a $\sim 1.2 M_{\odot}$ binary that has been orbiting the cluster and suffering the effects of dynamical friction for a significant fraction of the cluster lifetime. The efficiency of dynamical friction decreases for increasing radial distance from the centre, as a function of the local velocity dispersion and mass

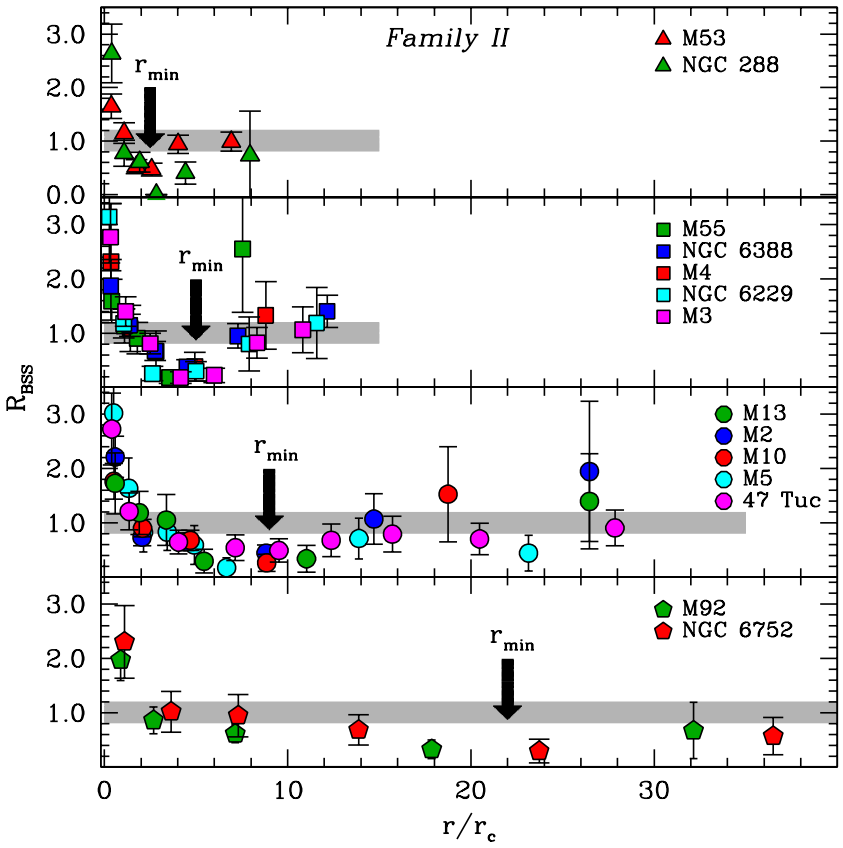

Fig. 5.11 BSS radial distribution observed in clusters of intermediate dynamical age (*Family II*). The distribution is clearly bimodal and the radial position of the minimum (marked with the arrow and labelled as $r_{\rm min}$) clearly moves outward from top to bottom, suggesting that the bottom clusters are more dynamically evolved than the upper ones. For the sake of clarity, the grey bands schematically mark the distribution of the reference populations. From [32].

density. Hence, dynamical friction first segregates (heavy) objects orbiting close to the centre and produces a central peak in their radial distribution. As the time goes on, the effect extends to larger and larger distances, thus yielding to a region devoid of these stars (i.e., a dip in their radial distribution) that progressively propagates outward. Simple analytical estimate of the radial position of this dip turned out to be in excellent agreement with the position of the minimum in the *observed* BSS radial distributions ($r_{\rm min}$), despite a number of crude approximation (see, e.g., [54]). Moreover, a progressive outward drift of $r_{\rm min}$ as a function of time is confirmed by the results of direct N-body simulations that follow the evolution of ~ 1.2 M$_\odot$ objects within a reference cluster over a significant fraction of its lifetime.

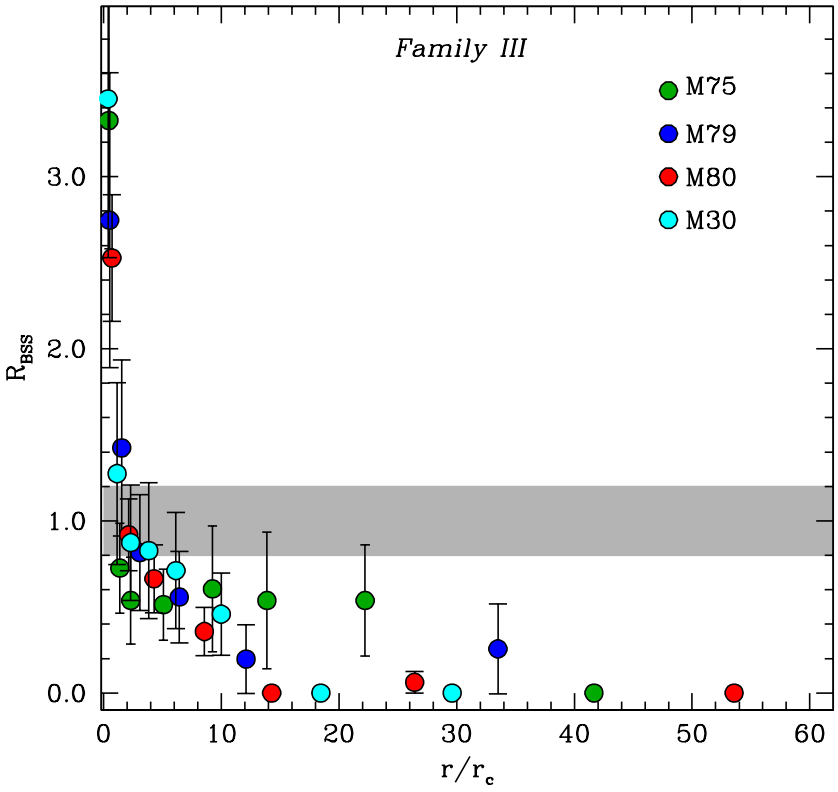

Fig. 5.12 BSS radial distribution for dynamically old clusters (*Family III*): only a central peak is visible, while the external upturn is no more present because, within the proposed scenario, the dynamical friction has been efficient out to the cluster outskirts. From [32].

In light of these considerations, the three families defined in Figs. 5.10–5.12 correspond to GCs of increasing dynamical ages. Hence, the shape of the BSS radial distribution turns out to be a powerful dynamical-age indicator. A flat BSS radial distribution (consistent with that of the reference population; see *Family I* in Fig. 5.10) indicates that dynamical friction has not played a major role yet even in the innermost regions, and the cluster is still dynamically young. This interpretation is confirmed by the absence of statistically significant dips in the BSS distributions observed in dwarf spheroidal galaxies ([55, 62]; see also Chap. 6): these are, in fact, collisionless systems where dynamical friction is expected to be highly inefficient. In more evolved clusters (*Family II*), dynamical friction starts to be effective and to segregate BSSs that are orbiting at distances still relatively close to the centre: as a consequence, a peak in the centre and a minimum at small radii appear in the distri-

bution, while the most remote BSSs are not yet affected by the action of dynamical friction (this generates the rising branch of the observed bimodal BSS distributions; see upper panel in Fig. 5.11). Since the action of dynamical friction progressively extends to larger and larger distances from the centre, the dip of the distribution progressively moves outward (as seen in the different groups of *Family II* clusters; Fig. 5.11, panels from top to bottom). In highly evolved systems dynamical friction already affected even the most remote BSSs, which started to gradually drift toward the centre: as a consequence, the external rising branch of the radial distribution disappears (as observed for *Family III* clusters in Fig. 5.12). All GCs with a single-peak BSS distribution can therefore be classified as "dynamically old".

Interestingly, this latter class includes M30 (see Section 5.4), a system that already suffered core collapse which is considered as a typical symptom of extreme dynamical evolution [60]. The proposed classification is also able to shed light on a number of controversial cases debated into the literature. In fact, M4 turns out to have an intermediate dynamical age, at odds with previous studies suggesting that it might be in a PCC state [36]. On the other hand, NGC 6752 turns out to be in a quite advanced state of dynamical evolution, in agreement with its observed double King profile indicating that the cluster core is detaching from the rest of the cluster structure [27]. Finally this approach might provide the key to discriminate between a central density cusp due to core collapse (as for M30) and that due to the presence of an exceptional concentration of dark massive objects (neutron stars and/or the still elusive intermediate-mass black holes; see the case of NGC 6388 in [43, 44], and references therein).

The quantisation in distinct age-families is of course an over-simplification, while the position of $r_{\rm min}$ is found to vary with continuity as a sort of clock time-hand. This allowed F12 to define the first empirical clock able to measure the dynamical age of a stellar system from pure observational quantities (the *dynamical clock*): as the engine of a chronometer advances the clock hand to measure the time flow, in a similar way the progressive sedimentation of BSSs towards the cluster centre moves $r_{\rm min}$ outward, thus marking its dynamical age. This is indeed confirmed by the tight correlations found between the clock-hand ($r_{\rm min}$) and the central and half-mass relaxation times ($t_{\rm rc}$ and $t_{\rm rh}$, respectively), which are commonly used to measure the cluster dynamical evolution time-scales. The trend with $t_{\rm rc}$ found by F12 is shown in Fig. 5.13 and the best-fit relations is:

$$\log(t_{\rm rc}/t_{\rm H}) = -1.11 \times \log(r_{\rm min}) - 0.78 \tag{5.2}$$

where $t_{\rm H}$ is the Hubble time. Note that, while $t_{\rm rc}$ and $t_{\rm rh}$ provide an indication of the relaxation timescales at specific radial distances from the cluster centre ($r_{\rm c}$ and $r_{\rm h}$, respectively), the dynamical clock here defined provides a measure of the global dynamical evolution of the systems, because the BSS radial distribution simultaneously probes all distances from the cluster centre.

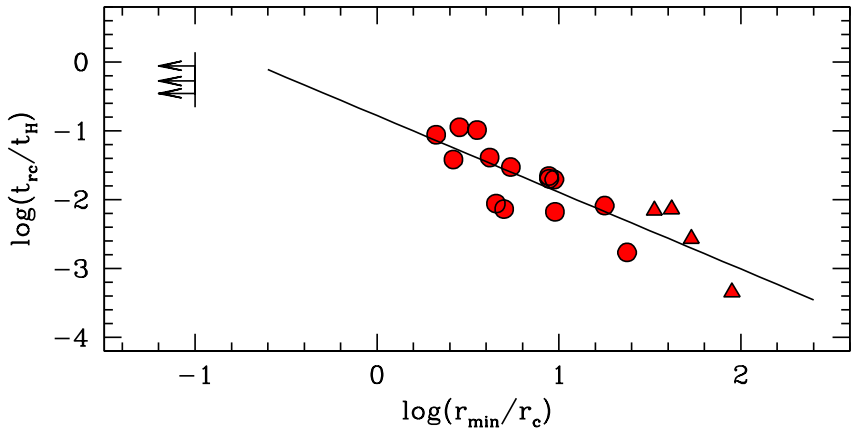

Fig. 5.13 Core relaxation time (normalised to the Hubble time t_H) as a function of the clock hand of the proposed *dynamical clock* ($r_{\rm min}$, in units of the core radius). Dynamically young systems (*Family I*) show no minimum and are plotted as lower-limit arrows at $r_{\rm min}/r_c = 0.1$. For dynamically old clusters (*Family III*, triangles), the distance of the farthest radial bin where no BSSs are observed has been adopted as $r_{\rm min}$. As expected for a meaningful clock, a tight anticorrelation is found: clusters with relaxation times of the order of the age of the Universe show no signs of BSS segregation (hence their BSS radial distribution is flat and $r_{\rm min}$ is not definable; see Fig. 5.10), whereas for decreasing relaxation times the radial position of the minimum increases progressively. The solid line correspond to the best-fit relations, given in (5.2). From [32].

5.7 Searching for the BSS Progeny: Evolved BSSs

Although BSSs have been routinely observed for 60 years now, no firm identification of even a single evolved BSS (E-BSS) has been obtained to date. Indirect evidence of the possible existence of E-BSSs has been derived from photometric criteria. Renzini & Fusi Pecci [68] suggested to search for E-BSSs during their core helium burning phase, when they should appear redder and brighter than *normal* HB stars, i.e. they should be located in a region of the CMD between the HB level and the Asymptotic Giant Branch (AGB). Following this prescription Fusi Pecci and collaborators [33] identified a few E-BSS candidates in several clusters with predominantly blue HBs, where the likelihood of confusing E-BSSs with true HB or evolved HB stars was minimised. Following the same prescription, F97 identified a sample of E-BSS candidates in M3 (see upper panel in Fig. 5.14), demonstrating that their radial distribution is similar to that observed for BSSs (see lower panel in Fig. 5.14 and Fig. 5.9). Similar results have been obtained by us [25] in the case of M80 (Fig. 5.15). The cumulative distribution of E-BSSs is consistent with that of BSSs and significantly different from that of genuine HB+RGB stars. Indeed, the Kolmogorov-Smirnov probability that E-BSSs and BSSs are extracted from the same parent population is $\sim 67\%$, while the same probability between E-BSSs and

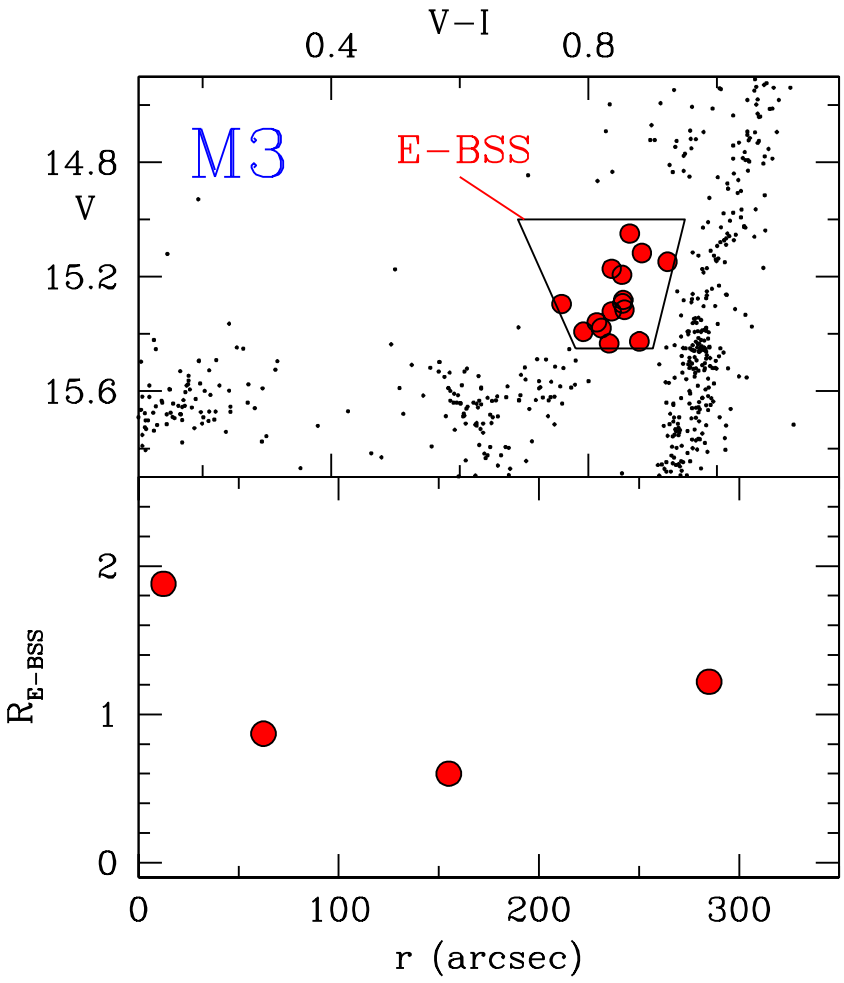

Fig. 5.14 *Upper panel*: CMD of M3 zoomed in the HB/AGB region. Red circles and the box mark the sample of candidate evolved BSSs. *Lower panel*: Double normalised ratio computed for the sample of candidate E-BSSs. A bimodality similar to that found for BSSs (see Fig. 5.9) is clearly visible. From [24].

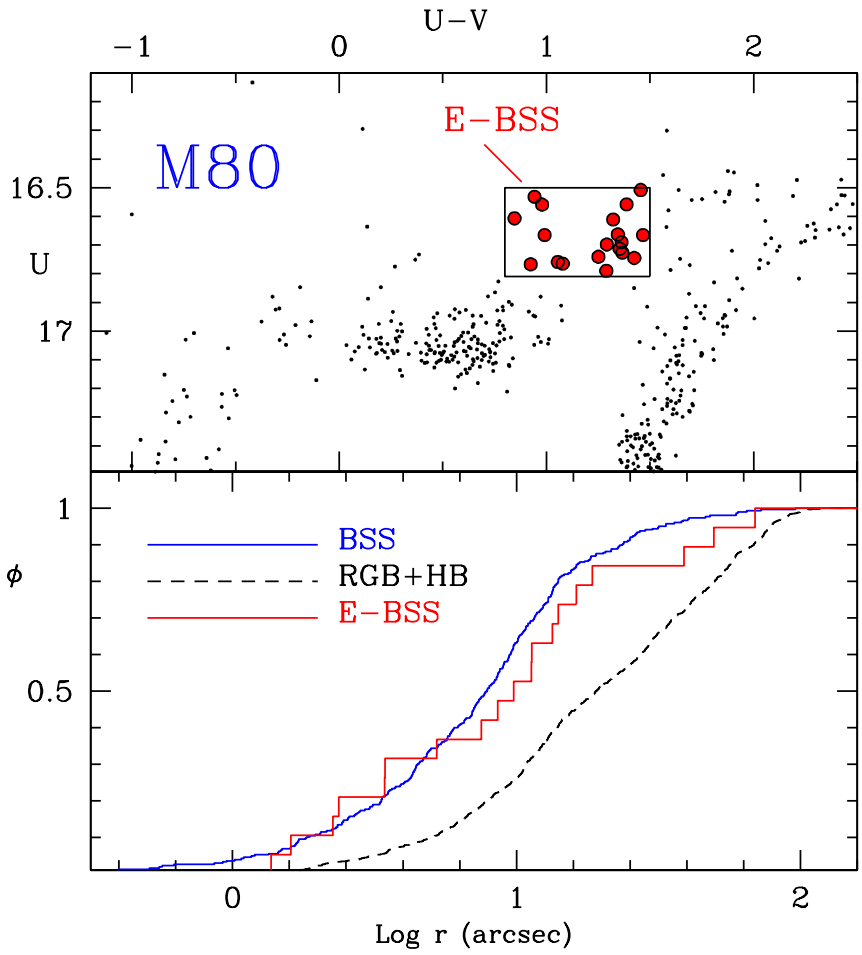

Fig. 5.15 *Upper panel*: CMD of M80 zoomed in the HB/AGB region. Red circles and the box mark the sample of candidate evolved BSSs. *Lower panel*: Cumulative radial distribution of BSSs (blue line), RGB+HB stars (black dashed line) and candidate evolved BSSs (red line). Clearly, E-BSSs share the same radial distribution of BSSs and are significantly more segregated than normal cluster stars (RGB and HB stars). From [25].

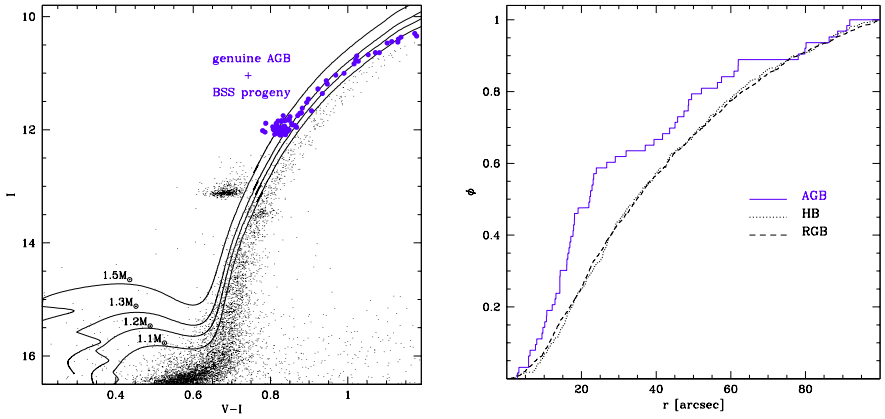

Fig. 5.16 *Left panel*: Portion of the CMD of 47 Tucanae above the MS-TO. Blue circles highlight the AGB population, which is suspected to be severely contaminated by a sample of E-BSSs. Solid lines are theoretical tracks from Pietrinferni et al. [65] for stars with masses ranging between 1.1 $M_{\odot}$ and 1.5 $M_{\odot}$ (see labels), showing that the RGB phase of these massive objects is well superposed to the AGB sequence of the cluster. *Right panel*: Cumulative radial distribution of the AGB population, likely contaminated by E-BSSs (blue solid line), compared to that of HB stars (black dotted line) and RGB stars (black dashed line). Clearly, the "AGB" population is significantly more segregated than normal cluster stars, as expected if it is contaminated by more massive objects, as E-BSSs. From [4].

RGB stars decreases to only $\sim 1.6\%$. This result confirms the expectation that E-BSSs share the same radial distribution of BSSs, both being more massive than the bulk of the cluster stars. It is interesting to note that the ratio between the number of bright BSSs and that of E-BSSs is $N_{\rm bBSS}/N_{\rm EBSS} \approx 6.5$ in both GCs [24, 25]. An approximate estimate of the lifetime ratio between BSSs (i.e., BSSs in the MS evolutionary stage) and their progeny can be obtained from the ratio between the total number of BSSs and that of E-BSSs. This turns out to range between 11 and 16, thus suggesting that we should expect 1 E-BSS ever 13 genuine BSSs. Indeed this is in very good agreement with the predictions of recent theoretical models of E-BSSs [77].

More recently, we [4] discovered a very promising signature of the existence of BSS descendants along the AGB of 47 Tuc: a *significant excess* of stars which are *more centrally segregated* than the RGB and HB populations has been found in the AGB region of the CMD (Fig. 5.16). Within $1'$ from the cluster centre ~ 53 "AGB stars" are counted, while only ~ 38 such objects are predicted on the basis of the HB star number counts and the post-MS evolutionary timescales [68]: this makes an excess of $\sim 40\%$! Because of the typical low stellar mass along the AGB ($M \sim 0.6$ $M_{\odot}$), this feature is hardly understandable in terms of a mass segregation effect on these stars. Instead it is very likely due to a sample of more massive objects, that, given the large population of BSSs in 47 Tuc, most probably are the BSS descen-

dants. Indeed, the comparison with theoretical tracks [65] and collisional models [77] shows that the AGB population of 47 Tuc can be significantly contaminated by stars with masses typical of BSSs (between $\sim$ 1.1 and $\sim$ 1.6 $M_{\odot}$), which are currently experiencing the first ascending RGB (Fig. 5.16).

These photometric indications are very promising. Ongoing spectroscopic follow-ups of E-BSS candidates selected in these three clusters will allow the first clear cut detection of the BSS progeny. Indeed due to their higher mass, E-BSSs are expected to be distinguishable from genuine AGB stars on the basis of their higher values of the surface gravity. Also their rotational and chemical composition will be measured, thus providing the first ever collected information about the physical properties of these peculiar stars during evolutionary paths subsequent to the core hydrogen burning phase. In turn, these are new, precious ingredients for the current and future theoretical modeling of these exotica.

5.8 Chemical and Kinematical Properties of BSSs

Theoretical models still predict conflicting results on the expected properties of BSSs generated by different production channels. In fact, high rotational velocities are expected for both MT-BSSs [73] and COL-BSSs [7], but braking mechanisms like magnetic braking or disk locking have been suggested to subsequently slow down the stars, with timescales and efficiencies which are still unknown [48, 76]. Concerning the chemical surface abundances, hydrodynamic simulations [49] have shown that very little mixing is expected to occur between the inner cores and the outer envelopes of the colliding stars. On the other hand, signatures of mixing with incomplete CN-burning products are expected at the surface of BSSs formed via the MT channel, since the gas at the BSS surface is expected to come from deep regions of the donor star, where the CNO burning occurred [73].

Sparse spectroscopic observations provided the first set of physical properties of BSSs (effective temperature, mass, rotation velocity, etc.; see [17]), but a systematic survey of basic parameters and surface abundance patterns was lacking, particularly in GCs. Recently, extensive campaigns with multiplexing spectrographs mounted at 8-m class telescopes (as *FLAMES* at the *ESO-VLT*) allowed to measure the chemical and kinematic properties for representative numbers of BSSs in a sample of Galactic GCs. The selected clusters differ in dynamical state, metallicity and density, thus providing an ideal sample for testing any possible link between the properties of BSSs and those of the host cluster. Indeed these observations represent a gold mine of information, providing the first characterisation of the structural properties of BSSs in GCs.

The first results of this search have lead to an exciting discovery: by measuring the surface abundance patterns of 43 BSSs in 47 Tuc, we [30] discovered a sub-population of BSSs with a significant depletion of carbon and oxygen, with respect to the dominant population (see Fig. 5.17). This evidence is interpreted as the presence of CNO burning products on the BSS surface, coming from the core of a deeply

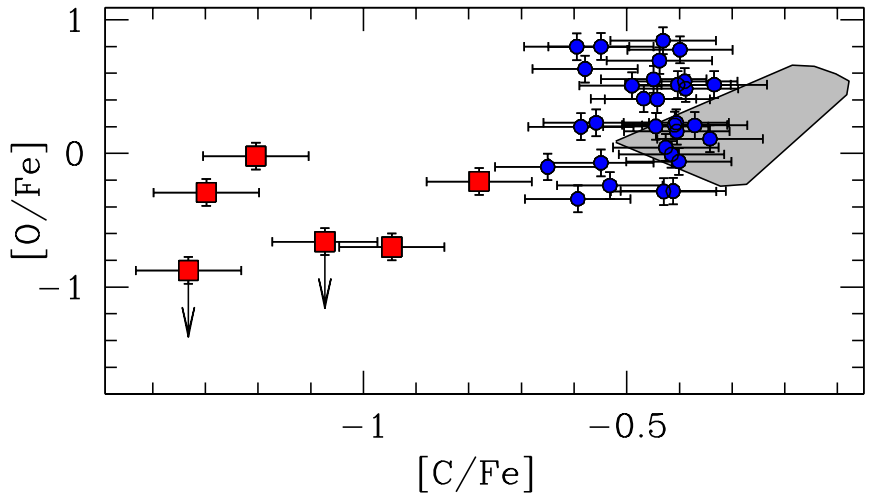

Fig. 5.17 [O/Fe] ratio as a function of [C/Fe] for the sample of 43 BSSs observed in 47 Tuc. Normal BSSs are marked with blue circles, while CO-depleted BSSs are marked with filled red squares. The gray region corresponds to the location of the 12 TO stars analyzed by [11]. From [30].

peeled parent star, as expected in the case of the MT formation channel. Thus, such a discovery in 47 Tuc could be the first detection of a chemical signature clearly pointing to the MT formation process for BSSs in a GC. Moreover, these observations have shown that (1) most of the BSSs are slow rotators; (2) the CO-depleted BSSs and the few BSSs with $v \sin i > 10$ km/s appear to be "less evolved" than the others: they all lie within a narrow strip at the faint-end of the BSS luminosity distribution in the CMD (see Fig. 5.18); (3) some of them are W UMa binaries, further suggesting that the evolution of these systems could be a viable channel for the formation of BSSs in GCs.

Which is the scenario emerging from these observations? In the early stage of mass transfer in W UMa systems (*Stage-1*), unprocessed material could be transferred and the resulting star would have normal C-O abundances (see Fig. 5.19). As the transfer continues, the accreted material could come from regions processed by the CNO cycle. Hence, first C and then both C and O would appear depleted (*Stage-2*). Thus it is possible to find depleted C, normal O BSSs/W UMa stars. After the merger, the star would appear as a CO-depleted non-variable BSS (*Stage-3*). In the sample studied in 47 Tuc, two or three BSSs are found in *Stage-2*, and 4 in *Stage-3*. The number of BSSs with CO depletion and the presence of W UMa systems show that the MT channel is active even in a high-density cluster like 47 Tuc: at least 15% of the BSSs are being produced by MT.

The distribution of rotational velocities provide additional clues to this scenario. In fact, most BSSs in the 47 Tuc sample are slow rotators [30], with velocities com-

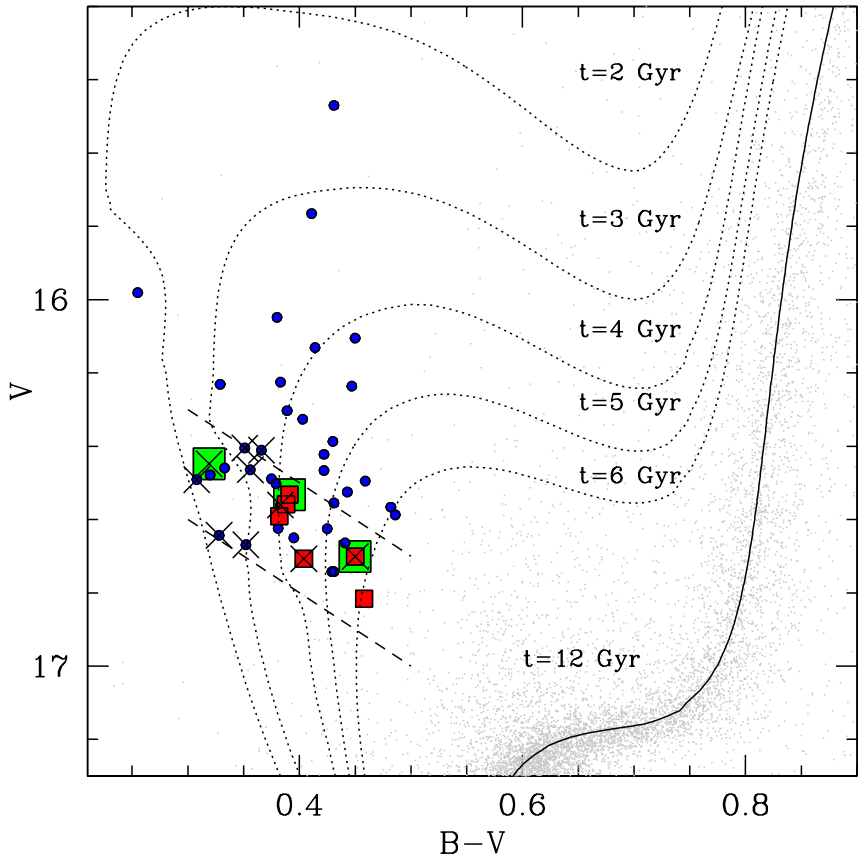

Fig. 5.18 CMD of 47 Tuc zoomed in the BSS region. BSSs showing no chemical anomalies are marked with blue circles, while CO-depleted BSSs are shown as red squares. Isochrones of different ages (from 2 to 12 Gyr) from [10] are overplotted for comparison. The three W UMa systems and the 10 BSSs rotating with $v \sin i > 10$ km/s are highlighted with large green squares and large crosses, respectively.

patible with those measured in unperturbed TO stars [52]. In particular, among the three BSSs identified as W UMa systems, one is found to be a rapid rotator and two are intermediate-slow rotators. This seems at odds with what is expected, especially for W UMa systems which are predicted to be rapid rotators, but, of course, different inclination angles may play a role. In any case, from their location in the CMD, all the fastest BSSs are presumedly the most recently born (see Fig. 5.18). This is also the region of C-O depletion and the W UMa behavior. The cooler, older BSSs rotate more slowly and have "normal" C-O abundances. Hence, this might suggest that during the evolution some mixing occurred and the rotation slows down. While ro-

tational mixing ordinarily increases CNO anomalies, in MT-BSSs the C-O depleted material overlies the material with normal abundances and chemical anomalies are therefore reduced. C and possibly O would still be low, but less so than a MT-BSS at birth. Indeed, the bulk of the 47 Tuc sample has C roughly one half of that of the TO stars (however, this could be due to systematics, since C in TO stars has been measured from different lines with respect to BSSs). Future observations will hopefully clarify this issue.

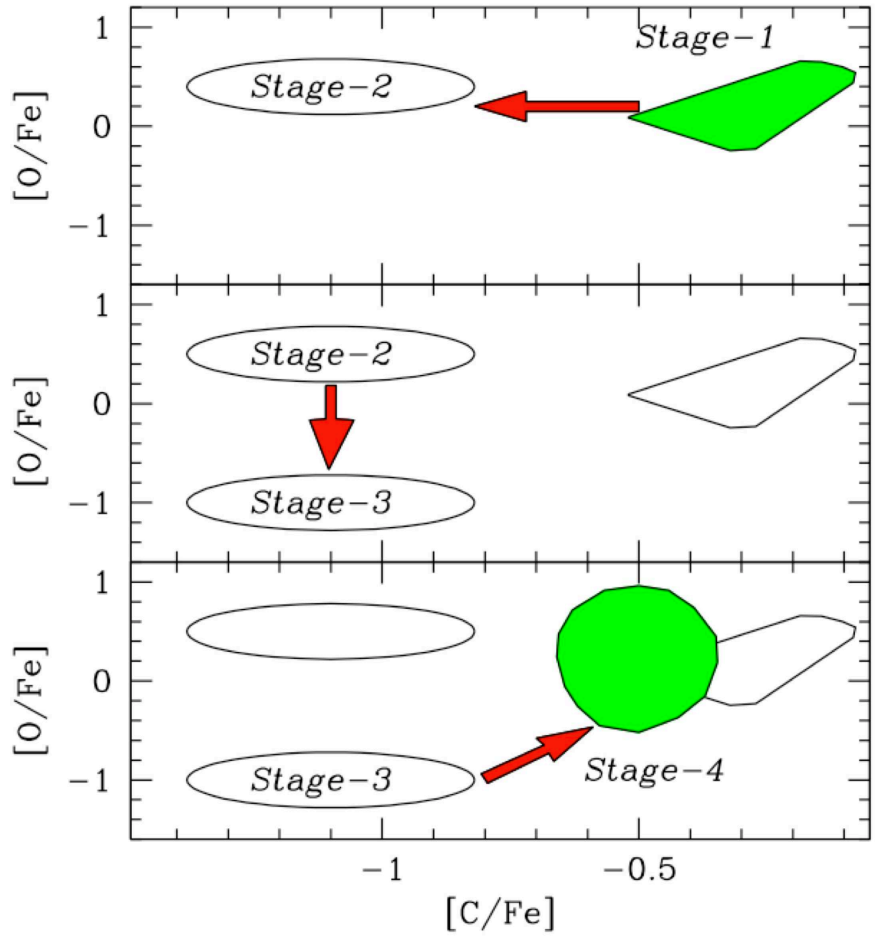

Fig. 5.19 Suggested evolution of BSSs in the [O/Fe]-[C/Fe] diagram. The four different stages discussed in the text are shown.

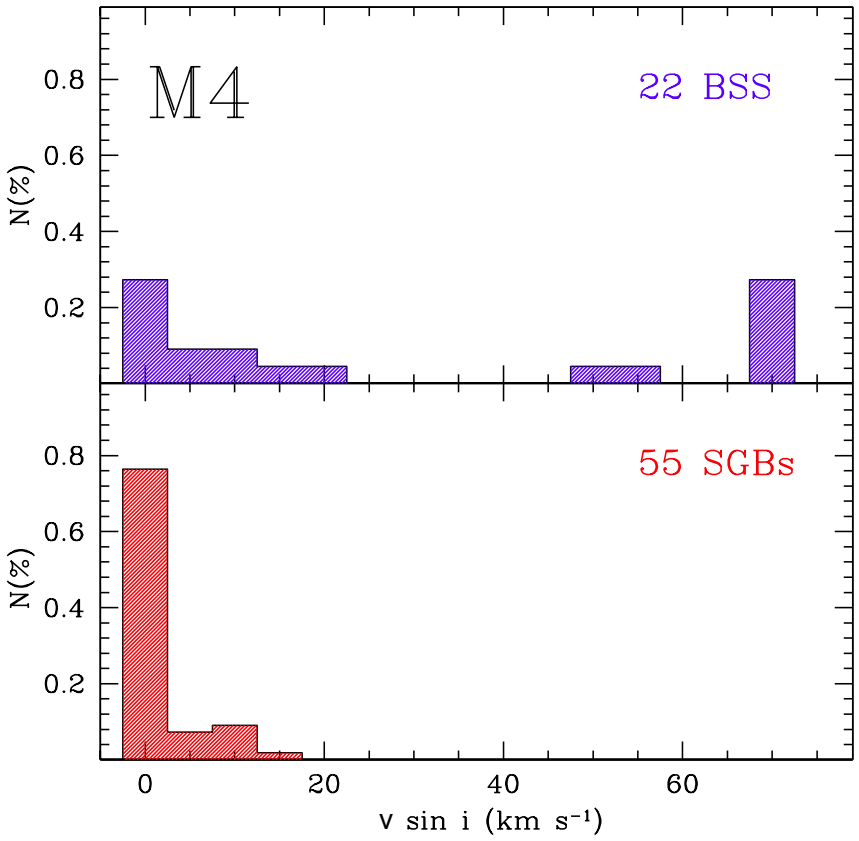

Fig. 5.20 Distribution of rotational velocities measured for 22 BSSs (upper panel) and 55 SGB stars (lower panel) in the GC M4. Six BSSs have $v \sin i \geq 70$ km/s and are all plotted in a single bin. Eight BSSs have been classified as fast rotators (i.e., with $v \sin i > 50$ km/s) and represent the largest sample (40% of the total) of rapidly rotating BSSs ever measured in a GC. From [50].

A similar study has now been extended to other clusters and up to now more than 160 BSSs in 5 GCs (namely 47 Tuc, M4, NGC 6397, M30 and ωCen) have been observed ([30, 50, 51], Mucciarelli et al. 2013 in preparation). Unfortunately, however, these observations provided the first observational evidence that radiative levitation affects not only HB stars hotter than 11,000 K [67], but also BSSs hotter than $T > 8,000$ K [51]. The effect is clearly traced by the value of the metallicity measured on the surface of the hottest BSSs, which is systematically and significantly larger than that of the parent cluster [51]. Of course, in presence of radiative levitation the measured chemical abundances cannot be interpreted in the context of the BSS formation channels and the occurrence of this process in the hottest (and

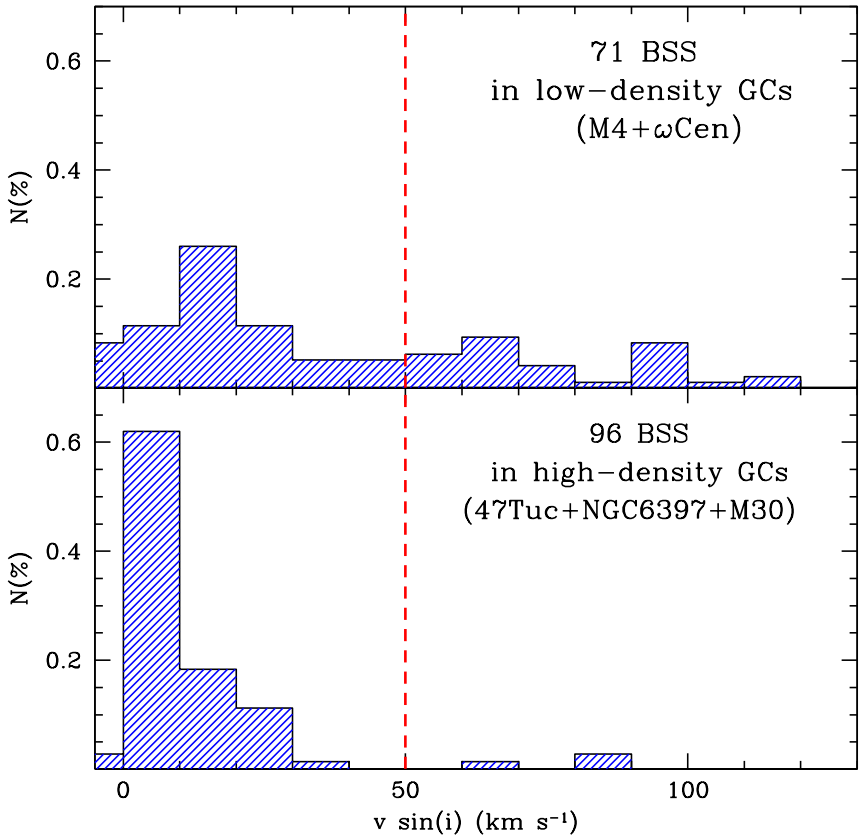

Fig. 5.21 Distribution of rotational velocities of 71 BSSs observed in low-density GCs (upper panel) and 96 BSSs in high-density GCs (lower panel). A systematic difference is apparent, possibly suggesting that some braking mechanism is active in high-density environments, while rapid rotation can last longer in low-density clusters. Adapted from [50, 51].

brightest) BSSs has *de facto* hampered the possibility of putting the result found in 47 Tuc onto a more solid statistical base. In fact the observable pool of "safe BSSs" (i.e. those cooler than 8000 K) is quite limited in number, or too faint for the capabilities of the current generation of high-resolution spectrographs ($V \lesssim 18-18.5$). The results obtained from the few BSSs not affected by radiative levitation are the following: no chemical anomalies have been found in the sample of 11 BSSs measured in M4 [50], only one depleted BSS has been found in M30 (Lovisi et al. 2013, ApJ submitted), and possibly one or two have been observed in ω Centauri (Mucciarelli et al. 2013, in prep.). Within the limitations of small number statistics, the collected data confirm that the percentage of CO-depleted BSSs is small (of the order of 10%), thus indicating either that CO-depletion is only temporarily visible on

the BSS surface (and then it is cleaned up by the subsequent evolution), or that the specific formation channel generating this feature has a limited efficiency in GCs.

A quite intriguing result seems instead to emerge from the measurement of the BSS rotational velocities: in M4, we [50] found that $\sim 40\%$ of the measured BSSs are fast rotators, with rotational velocities $v \sin i > 50$ km/s (see Fig. 5.20). *This is the largest frequency of rapidly rotating BSSs ever detected in a GC.* Interesting enough, while a similar fraction has been found in ω Cen (Mucciarelli et al. 2013, in prep.), significantly different results have been found in 47 Tuc, NGC 6397 and M30, where almost all ($92\% - 94\%$) BSSs rotate slowly ($v \sin i < 20$ km/s [30, 51]). These results suggest a possible correlation between the total fraction of rapidly spinning BSSs and the density of the host cluster: in fact, GCs with the largest fraction of fast rotators are also the loosest in our sample ($\log \rho_0 = 3.91$ and 3.43 in units of $M_\odot/pc^3$ for M4 and ω Cen, compared to $\log \rho_0 = 5.20$ for 47 Tuc and the very high central densities of the PCC clusters NGC 6397 and M30; [59]). The total fraction of fast rotating BSSs in the M4+ω Cen sample is $\sim 33\%$, whereas it is only $\sim 4\%$ in the higher-density sample of 47 Tuc+NGC 6397+M30 (see Fig. 5.21). If confirmed, this would be the first evidence of a direct link between the BSS physical properties and the characteristics of the host cluster, and it could lead to interesting scenarios never explored before. These results indicate that some braking mechanism (either magnetic braking or disk locking, as proposed by Leonard & Livio [48] and Sills, Adams & Davies [76], or something different/additional) could somehow depend on the parent cluster environment. For instance, recurrent stellar interactions might be efficient in decreasing the BSS rotational velocities, while in loose GCs, where stellar interactions are less frequent, the initial rotational velocities of BSSs might be preserved and a larger fraction of fast rotators should be observable.

While the mystery of BSS formation is not completely solved yet, detailed photometric and spectroscopic observations of these puzzling stars are providing crucial information about their physical properties, also shedding new light on the global dynamical evolution of stellar systems.

Acknowledgements Most of the results discussed in this chapter have been obtained within the project *Cosmic-Lab* (PI: Ferraro, see `http://www.cosmic-lab.eu`), a 5-year project funded by the European European Research Council under the 2010 *Advanced Grant* call (contract ERC-2010-AdG-267675). We warmly thank the other team members involved in this research: Giacomo Beccari, Paolo Miocchi, Mario Pasquato, Nicoletta Sanna and Rodrigo Contreras Ramos. The authors dedicate this chapter to the memory of Bob Rood, a pioneer in the theory of the evolution of low mass stars and a dear friend who shared our enthusiasm for the BSS topic and who unexpectedly passed away on 2 November 2011.

References

1. Anderson, J.: Omega Centauri, A Unique Window into Astrophysics, ASP 265, 87 (2002)
2. Auriere, M., Lauzeral, C., Ortolani, S.: Nature **344**, 638 (1990)
3. Bailyn, C. D.: A&ARA **33**, 133 (1995)

4. Beccari, G., Ferraro, F. R., Lanzoni, B., Bellazzini, M.: ApJL **652**, L121 (2006)
5. Beccari. G., et al.: ApJ **679**, 712 (2007)
6. Beccari, G., Sollima, A., Ferraro, F. R., et al.: ApJL **737**, L3 (2011)
7. Benz, W., Hills, J. G.: ApJ **323**, 614 (1987)
8. Bolte, M., Hesser, J. E., Stetson, P. B.: ApJL **408**, L89 (1993)
9. Buonanno, R., Corsi, C.E., Buzzoni, A., Cacciari, C., Ferraro, F.R., Fusi Pecci, F.: A&A **290**, 69 (1994)
10. Cariulo, P., Degl'Innocenti, S. Castellani, V.: A&A **412**, 1121 (2003)
11. Carretta, E., Gratton, R. G., Lucatello, S., Bragaglia, A., Bonifacio, P.: A&A **433**, 597 (2005)
12. Contreras Ramos, R., Ferraro, F. R., Dalessandro, E., Lanzoni, B., Rood, R. T.: ApJ **748**, 91 (2012)
13. Dalessandro, E., et al.: A&A **677**, 1069 (2008a)
14. Dalessandro, E., et al.: A&A **681**, 311 (2008b)
15. Dalessandro, E., Ferraro, F. R., Massari, D., et al.: ApJ **778**, 135 (2013)
16. Davies, M. B., Piotto, G., de Angeli, F.: MNRAS **349**, 129 (2004)
17. De Marco, O., et al.: ApJ **632**, 894 (2005)
18. Djorgovski, S., Meylan, G.: Structure and Dynamics of Globular Clusters, ASP 50, 325 (1993)
19. Djorgovski, S., King, I. R.: ApJL **305**, L61 (1986)
20. Dotter, A., Sarajedini, A., Yang, S.-C.: AJ **136**, 1407 (2008)
21. Ferraro, F. R., Paresce, F.: AJ **106**,154 (1993)
22. Ferraro F. R., Pecci F. F., Cacciari C., Corsi C., Buonanno R., Fahlman G. G., Richer H. B.: AJ **106**, 2324 (1993)
23. Ferraro, F. R., Fusi Pecci, F., Bellazzini, M.: A&A **294**, 80 (1995)
24. Ferraro, F. R., et al.: Paltrinieri, B., Fusi Pecci, F., Cacciari, C., Dorman, B., Rood, R. T., Buonanno, R., Corsi, C. E., Burgarella, D., Laget, M.: A&A **324**, 915 (1997; F97)
25. Ferraro, F. R., Paltrinieri, B., Rood, R. T., Dorman, B.: ApJ **522**, 983 (1999a)
26. Ferraro, F. R., Sills, A., Rood, R. T., Paltrinieri, B., Buonanno, R. : ApJ **588**, 464 (2003)
27. Ferraro, F. R., Possenti, A., Sabbi, E., et al.: ApJ **595**, 179 (2003)
28. Ferraro, F. R., Beccari, G., Rood, R. T., Bellazzini, M., Sills, A., Sabbi, E.: ApJ **603**, 127 (2004)
29. Ferraro, F. R., Sollima, A., Rood, R. T., Origlia, L., Pancino, E., Bellazzini, M.: ApJ **638**, 433 (2006a)
30. Ferraro, F. R., et al.: A&A **647**, L53 (2006b)
31. Ferraro, F. R., Beccari, G., Dalessandro, E., et al.: Nature **462**, 1028 (2009; F09)
32. Ferraro, F. R., Lanzoni, B., Dalessandro, E., et al.: Nature **492**, 393 (2012; F12)
33. Fusi Pecci, F., Ferraro, F. R., Corsi, C. E., Cacciari, C., Buonanno, R.: ApJ **104**, 1831 (1992)
34. Guhathakurta, P., Yanny, B., Bahcall, J. N., Schneider, D. P.: ApJ **108**, 1786 (1994)
35. Gilliland, R. L., Bono, G., Edmonds, P. D., et al.: ApJ **507**, 818 (1998)
36. Heggie, D. C., Giersz, M.: MNRAS **389**, 1858 (2008)
37. Hills, J. G., Day, C. A.: ApJL **17**, 87 (1976)
38. Jordi, K., Grebel, E. K., Hilker, M., et al.: AJ **137**, 4586 (2009)
39. Knigge, C., Leigh, N., Sills, A.: Nature **457**, 288 (2009)
40. Lanzoni, B., Dalessandro, E., Ferraro, F. R., Mancini, C., Beccari, G., Rood, R. T., Mapelli, M., Sigurdsson, S. : ApJ **663**, 267 (2007a)
41. Lanzoni, B., et al.: A&A **663**, 1040 (2007b)
42. Lanzoni, B., et al.: ApJ **670**, 1065 (2007c)
43. Lanzoni, B., Dalessandro, E., Ferraro, F. R., et al.: ApJL **668**, L139 (2007)
44. Lanzoni, B., Mucciarelli, A., Origlia, L., et al.: ApJ **769**, 107 (2013)
45. Leigh, N., Sills, A., Knigge, C.: ApJ **661**, 210 (2007)
46. Leigh, N., Sills, A., Knigge, C.: MNRAS **415**, 3771 (2011)
47. Leigh, N., Knigge, C., Sills, A., et al.: MNRAS **428**, 897 (2013)
48. Leonard, P. J. T., Livio, M.: ApJL **447**, 121 (1995)
49. Lombardi, J. C. Jr., Rasio, F. A., Shapiro, S. L.: ApJL **445**, 117 (1995)
50. Lovisi, L., Mucciarelli, A., Ferraro, F. R., et al.: ApJL **719**, 121 (2010)
51. Lovisi, L., Mucciarelli, A., Lanzoni, B., et al.: ApJ **754**, 91 (2012)

52. Lucatello, S., Gratton, R.G.: A&A **406**, L691 (2003)
53. Mapelli, M., Sigurdsson, S., Colpi, M., Ferraro, F. R., Possenti, A., Rood, R. T., Sills, A., Beccari, G.: ApJL **605**, 29 (2004)
54. Mapelli, M., Sigurdsson, S., Ferraro, F. R., Colpi, M., Possenti, A., Lanzoni, B.: MNRAS **373**, 361 (2006)
55. Mapelli, M., Ripamonti, E., Battaglia, G., et al.: MNRAS **396**, 1771 (2009)
56. Marín-Franch, A., Aparicio, A., Piotto, G., et al.: ApJ **694**, 1498 (2009)
57. Mathieu, R. D., Geller, A. M.: Nature **462**, 1032 (2009)
58. McCrea, W. H.: MNRAS **128**, 147 (1964)
59. McLaughlin, D. E., van der Marel, R. P.: A&A **161**, 304 (2005)
60. Meylan, G., Heggie, D. C.: A&A Rev. **8**, 1 (1997)
61. Milone, A. P., Piotto, G., Bedin, L. R., et al.: A&A **540**, A16 (2012)
62. Monelli, M., Cassisi, S., Mapelli, M., et al.: ApJ **744**, 157 (2012)
63. Moretti, A., de Angeli, F., Piotto, G.: A&A **483**, 183 (2008)
64. Paresce, F., Meylan, G., Shara, M., et al.: Nature **352**, 297 (1991)
65. Pietrinferni, A., Cassisi, S., Salaris, M., Castelli, F.: ApJ **642**, 797 (2006)
66. Piotto, G., et al.: ApJ **604**, L109 (2004)
67. Quievy, D., Charbonneau, P., Michaud, G., Richer, J.: A&A **500**, 1163 (2009)
68. Renzini, A., Fusi Pecci, F.: A&ARA **26**, 199 (1988)
69. Sabbi, E., Ferraro, F. R., Sills, A., Rood, R. T.: ApJ **617**, 1296 (2004)
70. Sandage A. R.: AJ **58**, 61 (1953)
71. Sarajedini, A.: Blue Stragglers, ASP **53**, 14 (1993)
72. Sarajedini, A., Bedin, L. R., Chaboyer, B., et al.: AJ **133**, 1658 (2007)
73. Sarna, M. J., de Greve, J. P.: QJRAS **37**, 11 (1996)
74. Shara, M. M., Saffer, R. A., Livio, M.: ApJ **489**, L59 (1997)
75. Sigurdsson, S., Davies, M.B., Bolte, M.: ApJL **431**, 115 (1994)
76. Sills, A., Adams, T., Davies, M. B.: MNRAS **358**, 716 (2005)
77. Sills, A., Karakas, A., Lattanzio, J.: ApJ **692**, 1411 (2009)
78. Sollima, A. et al.: A&A **481**, 701 (2008)
79. Tian, B., Deng, L., Han, Z., Zhang, X. B.: A&A **455**, 247 (2006)
80. Warren, S. R., Sandquist, E. L., Bolte, M.: ApJ **648**, 1026 (2006)
81. Zaggia, S. R., Piotto, G. Capaccioli M.: A&A **327**, 1004 (1997)
82. Zinn, R., Searle, L.: ApJ **209**, 734 (1976)